ACS Energy LETTERS

http://pubs.acs.org/journal/aelccp

Advanced Impedance Analysis for Performance Degradation during Low-Temperature CO_2 Electroreduction

Qinhao Chen, Alexander Kube, Dennis Kopljar,* and Kaspar Andreas Friedrich*

Cite This: *ACS Energy Lett.* 2024, 9, 6096−6103

Read Online

ACCESS | Metrics & More | Article Recommendations | Supporting Information

ABSTRACT: **Electrochemical impedance spectroscopy (EIS) is a powerful tool commonly used to study electrochemical systems. Nevertheless, its application in CO_2 electroreduction has been so far limited due to its complex reaction mechanism and environment. Although initial findings have demonstrated the viability of applying EIS analysis in CO_2 electrolyzers, the assignment of individual processes in the impedance spectra remains ambiguous. Therefore, a more detailed investigation, especially focused on its application in evaluating degradation mechanisms, is essential. In this study, a stable gas diffusion electrode (GDE) system was developed for a comprehensive EIS and distribution of relaxation time (DRT) evaluation to assess key degradation mechanisms under accelerated stress conditions such as high current density and low operating temperature. Validated by post-mortem analysis and complementary methods, we demonstrate the viability of this approach for operando monitoring of CO_2 electroreduction by assigning individual mechanistic processes in the GDE and linking them to performance degradation over time.**

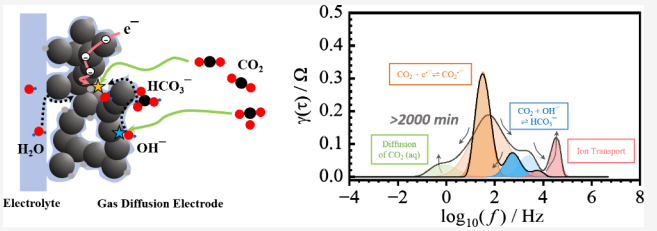

For the electrochemical reduction of CO_2 (CO2R) to be an economically viable solution to produce value-added chemicals on a commercial scale, an adequate long-term stability (several 1000 h) at state-of-the-art performance has to be demonstrated. While most academic studies have been focusing on achieving industrially relevant performance metrics (e.g., product distribution, current density, and polarization losses), attention needs to pivot toward the study of long-term stability in realistic systems and settings to advance the technology. For that purpose, distinctive testing protocols have been developed to evaluate the performance of CO2R systems based on Faradaic efficiency, working potential, applied current density,[1] and their evolution over time.[2] As for the stability assessment, the analysis of production distribution, ante- and post-mortem cyclic voltammetry for reactive surface area,[3,4] and potentiometry or amperometry measurements[5] have been typically applied. Furthermore, to obtain a better understanding on the material and component level, operando techniques (e.g., XPS, XAS, Raman, and IR), which monitor processes on the atomic- and molecular level,[6−8] and multiscale modeling[9] have been shown to give essential insights into reaction mechanisms and aid in the rational optimization of the system. However, none of the above techniques fulfill the requirements of giving information on degradation mechanisms while being simultaneously operando, nondestructive, and applicable on a large-scale test bench in an easy-to-operate manner.

Electrochemical impedance spectroscopy (EIS) is a technique that allows evaluating the performance of electrochemical systems while offering detailed insights into both physical and electrochemical processes[10] without disturbing or disrupting the investigated system. The drawback of EIS is that its application requires the construction of an adequate equivalent circuit model (ECM) for the analysis of the underlying processes. This requires significant knowledge of the system and is not unambiguous. To solve that issue, the distribution of relaxation times (DRT) has been used as a largely model-free analysis method which deconvolutes frequency domain data from EIS into a distribution of time constants, obtaining a separation of the total impedance into distinctive processes with enhanced spectral resolution.[11] Qu et al. and Sun et al. have nicely demonstrated the viability of using DRT analysis to diagnose an MEA-type zero-gap CO_2 electrolyzer during CO production for the first time.[12,13]

Received: September 27, 2024
Revised: November 5, 2024
Accepted: November 22, 2024
Published: November 26, 2024

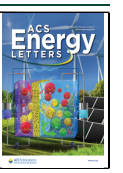

https://doi.org/10.1021/acsenergylett.4c02673
ACS Energy Lett. 2024, 9, 6096−6103

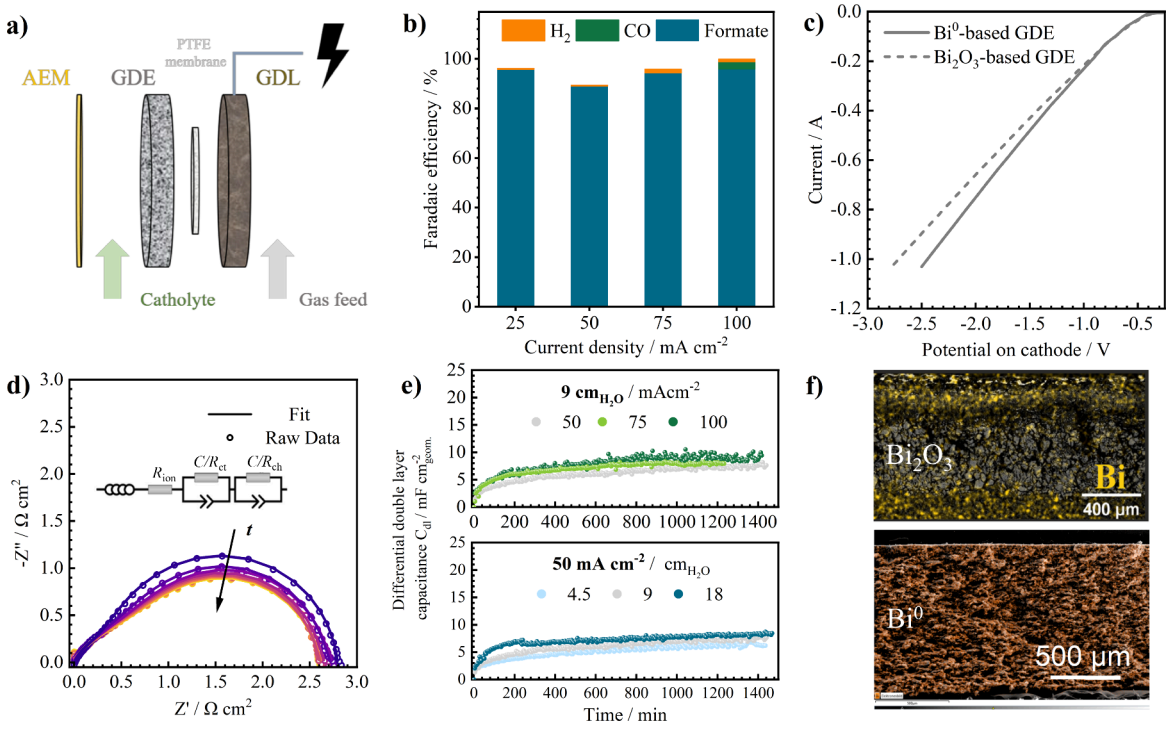

Figure 1. (a) Cathode configuration for the electrochemical and impedance analysis. (b) Faradaic efficiencies of Bi^0-based GDEs at various current densities. (c) Linear sweep voltammetry (LSV) of CO_2 electroreduction on the Bi^0- and Bi_2O_3-based GDEs. (d) Time evolution of impedance spectra (free of ohmic losses R_0) during CO2R with the proposed equivalent circuit. (e) C_{dl} of the charge transfer reaction (CO2R) retrieved in a three-electrode setup with different back pressures and applied current densities (water bath at 30 °C). (f) Post-mortem SEM/EDX element mapping of bismuth on the cross-sectional area of GDEs. Top: Bi_2O_3. Reproduced with permission from 5902731215468. Copyright 2024 Elsevier. Bottom: Bi.

However, although highly relevant and insightful, their analysis is partly obstructed by the superimposed nature of the processes that occur in the full cell. For a better understanding of what happens inside of the cathode GDE as a basis for a rational GDE design, the use of half-cells in three-electrode design is advantageous. This is particularly true for the investigation of degradation mechanisms related to potentially subtle factors that influence both kinetics and the different transport processes to varying degrees.[14] Furthermore, in liquid-electrolyte-based systems, various phenomena can limit performance, with carbonate formation and the wetting of the GDE structure by the liquid electrolyte being the most critical. For this application as well as for formate production, a combined EIS/DRT study has not been performed so far.

Motivated by the potential of impedance analysis as an operando method, our group (see Bienen et al.[15]) has conducted a comprehensive impedance spectroscopy study to unveil mechanistic processes of CO2R at a tin-based GDE and subsequently demonstrated the use of EIS to correlate the double-layer capacitance increase and electrode degradation during electrolysis.[16] However, it was difficult to separate short- and long-term degradation processes and to differentiate between catalyst- and electrode-related phenomena (e.g., flooding, catalyst redistribution, and physical erosion) due to the instability of both SnO_2 and to a certain degree Bi_2O_3.[16] As the main target of this work is to study the electrode-level processes that gradually alter the GDE performance over its lifespan on the cathode side and gain further understanding of this methodology, effects that could interfere with the processes of interest in the EIS spectra such as catalyst leaching, redistribution, and instantaneous flooding of the gas diffusion layer (GDL) need to be excluded beforehand.

Bismuth-based materials are known to be suitable catalysts to electrochemically reduce CO_2 to formate and are less prone to deactivation compared to, e.g., tin-based catalysts. However, commonly employed Bi_2O_3-based catalysts such as the one reported in our previous study experience dissolution and redeposition within the GDEs at negative working potentials[16−18] ($Bi_2O_3 + OH^- \rightleftharpoons 2BiO_2^- + H_2O$; $BiO_2^- + 2H_2O + 3e^- \rightleftharpoons Bi + 4OH^-$).

Thus, this process has impacts on the electrochemical behavior, which is observable in the EIS spectra and might superimpose other less dominant processes that build up over time and become relevant for long-term stability. To avoid this, a metallic Bi^0-based GDE was introduced herein based on the reduction of a bismuth−tartrate complex via sodium hypophosphite monohydrate[19] along with a specifically designed manufacturing procedure and its physical characterization (XRD, SEM/EDX) as illustrated in the SI (cf. Figures S1−S3). Besides that, the traditional electrode architecture that consists of a catalytic layer (CL) and a GDL in contact with the metallic current collector can limit long-term stability when a breakthrough of electrolyte from the CL into the GDL and a corresponding breakdown of electrolysis takes place. This is observable by an instantaneous change in the impedance spectra.[16] As we want to focus on the gradual degradation on the electrode-level during long-term electrolysis, the breakthrough of electrolyte was prevented by using an additional highly hydrophobic PTFE membrane placed in

https://doi.org/10.1021/acsenergylett.4c02673
ACS Energy Lett. 2024, 9, 6096−6103

between the reactive layer (here GDE) and the GDL. It allows gas transport but completely blocks liquid penetration (cf. Figure 1a). The area of the PTFE membrane corresponds to the active geometric area of GDE, while the electrical contact was ensured by the attachment of GDL with GDE in the area which is not covered by the PTFE membrane. For a realistic cell architecture, particularly in light of potential upscaling of the electrode dimension, this might not be a viable approach but rather serves as a measure to exclude superimposition of the investigated degradation phenomena by the instantaneous liquid breakthrough. The resulting Bi^0-GDEs were then tested in the above-mentioned setup for their general electrochemical performance of CO2R. As the results show, the investigated system is indeed comparable with the one based on Bi_2O_3 applied in our previous studies in terms of both the selectivity (cf. Figure 1b) and activity (cf. Figure 1c) of CO2R from low to medium current densities with almost exclusive production of formate.[16,20]

The impedance arcs (4.5 cm H_2O, 50 mA/cm^2) recorded at the early stage of the experiment represent a shrinking trend as the reaction goes on until a quasi-stationary stage is achieved where similar impedance spectra can be observed (cf. Figure 1d). The electrowetting process of Bi^0-GDEs during the long-term operation was then evaluated by fitting the impedance spectra with the equivalent circuit that consists of two RQ-elements representing the electron transfer process and the preceding chemical equilibrium of bicarbonate formation.[16,21] Consequently, C_{dl} can be derived using Brug's equation:[22] $C_{dl} = \left[Q\left(\frac{1}{R_\Omega} + \frac{1}{R_{ct}}\right)^{\alpha-1}\right]^{1/\alpha}$, where R_Ω stands for the ionic resistance and elements like the capacitance Q, reaction resistance R_{ct}, and exponential parameter α are the values of the RQ element retrieved from the fitting. In Figure 1e, C_{dl} experiences a sharp increase at the start of the experiment under all conditions, followed by a continuous rise along with decreasing overpotentials. This is due to the potential-dependent surface energy reduction at the electrolyte−GDE interface and continuous penetration of the electrolyte into the GDE[23] after the onset of the reaction. The overpotential gradually decreases due to an increase in the wetted catalyst surface area. After this electrowetting-in process, a quasi-stationary value of C_{dl} is obtained under various operating conditions. The change in C_{dl} aligns with observations from the impedance spectra. Additionally, the resulting value exhibits a positive correlation to the current density, i.e., the working potential, and the gaseous back pressure (cf. Table 1), which is qualitatively consistent with the Washburn equation.[24] By assessing the general electrowetting behavior from EIS spectra, we have confirmed that the developed GDE is physically and chemically stable under normal operating conditions. As can be seen from the SEM/EDX element mapping of bismuth from Figure 1f, the GDE based on Bi_2O_3 suffers from dissolution and redistribution within the GDE,[16] while the one based on metallic Bi is stable in alkaline solution. Importantly, the system is considered to be reliable and stable enough for subsequent EIS and DRT analysis.

Table 1. Quasi-Stationary C_{dl} Achieved at Different Applied Currents and Back Pressures

applied current density (mA·cm$^{-2}_{geo}$)	back pressure (cm H_2O)	quasi-stationary differential double-layer capacitance (mF·cm$^{-2}_{geo}$)	error bar (mF·cm$^{-2}_{geo}$)
50	9	6.45	±0.52
75	9	7.28	±0.44
100	9	8.90	±0.20
50	4.5	5.85	±0.44
50	9	6.45	±0.52
50	18	8.57	±0.71

By operating at stressed conditions (i.e., high current density and low feed temperature), the results of EIS, DRT analysis, and post-mortem characterization facilitate an assignment of the degradation mechanism commonly encountered in GDEs during CO2R. At a low operating temperature, carbonate precipitation as a result of the reaction between generated OH^- and dissolved CO_2 takes place faster within the electrodes during CO2R owing to the decreasing solubility of salts[25] and slower diffusion through the porous system into the bulk.[26] Based on that assumption and the relatively stable system introduced above, its long-term performance under a low operating temperature was comprehensively analyzed. As can be seen from the evolution of recorded impedance spectra (cf. Figure 2a), cathode potential, and product distribution (cf. Figures 3d and S4), the initial electrowetting-induced decrease in overpotential and reaction resistance is followed by a continuous rise in these parameters after a certain period, together with the onset of hydrogen production. In contrast, the system operating at room temperature at the same current density exhibits stable performance with negligible increase in reaction resistance (cf. Figure 2a) and hydrogen production (Table S2).

Post-mortem SEM/EDX was applied to evaluate precipitates on the electrode surface. At first, the electrode surface facing the electrolyte was rinsed by ultrapure water to remove the electrolyte KOH (cf. Figure S5a). Overall, results of SEM and EDX mapping (cf. Figure 2b, first row; Figure S5c) confirm catalyst leaching and changes in composition after long-term operation. The analysis suggests the formation of the bismuth subcarbonates ($(BiO)_4(OH)_2CO_3$ and $(BiO)_2CO_3$) on the GDE surface, which cannot be flushed away by water (in contrary to the potassium carbonates, which are dissolvable in water) but by diluted sulfuric acid (Figure S5b).[27] The accelerated carbonate precipitation process indicates a highly concentrated CO_3^{2-} environment by the chemical reaction between formed OH^- and dissolved CO_2 within the pore system, which leads to the formation of carbonates at a fast rate. Meanwhile, crystallite structures which can be observed from electrode cracks despite water rinsing suggest the occurrence of salt precipitation (K_2CO_3) inside the GDE within the electro-wetted area (cf. Figure 2b, second column). It is believed that such chemical and physical changes of the GDE cause an increase of the reaction and transport resistances, which is observed in the impedance spectra, as will be described in the following chapters.

To further study how carbonate precipitation and potential catalyst changes increase the reaction resistance and influence the impedance results, we took a closer look at the initial (9 min) and the last recorded impedance spectra (2214 min) after degradation at 75 mA/cm^2. Based on the mathematical relation between the ohmic resistance R_0, the polarization resistance R_{pol}, and the time constant τ according to $Z(\omega) = R_0 + \int_0^\infty \frac{g(\tau)}{1+j\omega\tau} d\tau$, DRT analysis was performed based on a Tikhonov regularization method implemented into the commercial software Relaxis.[11] The details about how

https://doi.org/10.1021/acsenergylett.4c02673
ACS Energy Lett. 2024, 9, 6096−6103

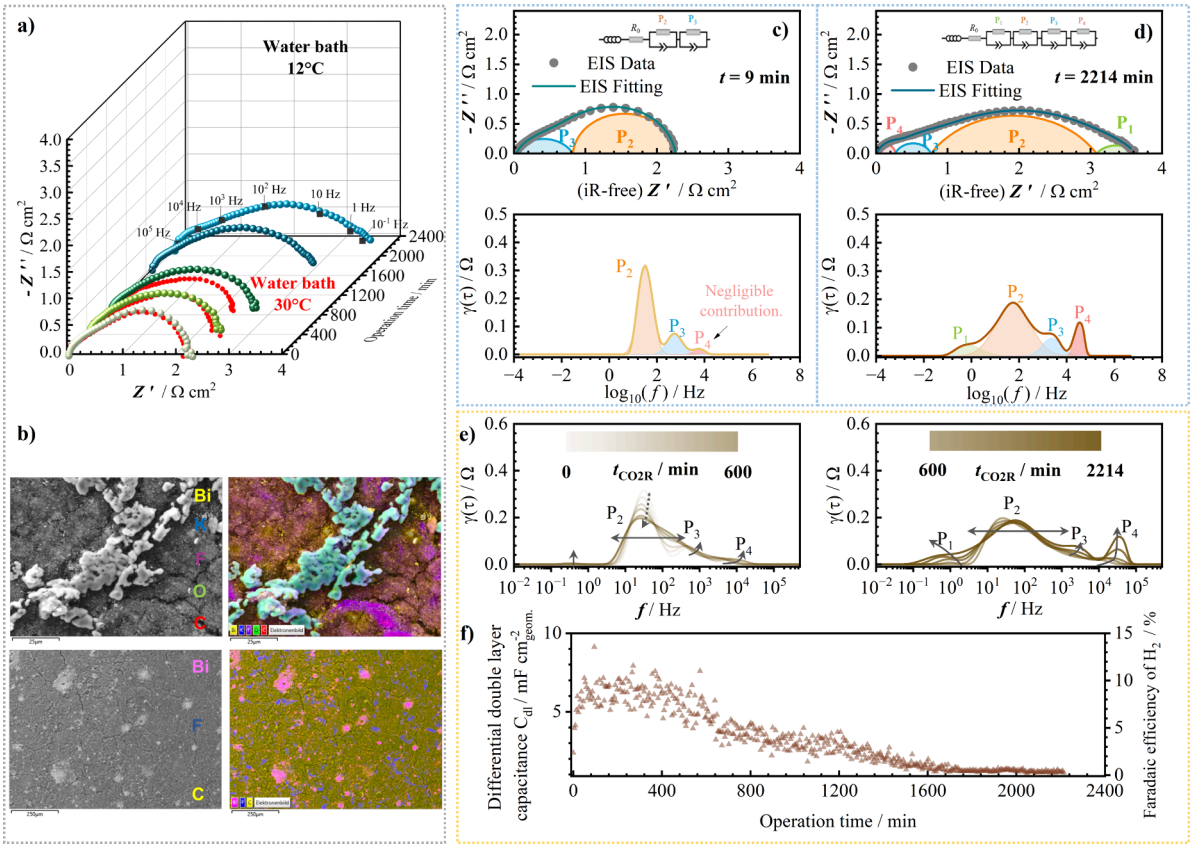

Figure 2. Condition: water bath 12 °C, 75 mA·cm^{-2}, gaseous backpressure 18 mbar$_g$. (a) Impedance spectra recorded over time (free of ohmic losses R_0) compared with the condition at 30 °C. (b) Post-mortem SEM images of the GDE surface flushed with ultrapure water (first column); EDX mapping focusing on emerging crystalline precipitates (second column). Measured and fitted impedance spectrum and DRT analysis at the start of (c) and the end of the measurement (d). (e) Computed DRT with identification of distinctive polarization processes over time. (f) C_{dl} retrieved from the fitting using two serial RQ elements.

DRT analysis was performed and the value choice of regularization factor λ to avoid noises in the frequency dispersion are described in the SI (cf. Figure S6), which is based on the L-curve method. As can be seen in Figure 2c, two major processes, P_2 and P_3, could be identified via DRT in the initial spectrum at 32 and 530 Hz, respectively.[15] This corresponds to the typical frequency range proposed for the charge transfer reaction ($CO_2 + e^{\bullet -} \rightleftharpoons CO_2^{\bullet -}$) and the chemical equilibrium of bicarbonate formation from CO_2 ($CO_2 + OH^- \rightleftharpoons HCO_3^-$), respectively. The reasoning for this assignment is based on a thorough impedance study and has been described in a previous publication by our group.[15] Although an additional process (P_4) was found at high frequency, it was not included in the equivalent circuit for the assessment of the initial spectrum owing to its small impedance contribution. In the end, the fitting results based on the initial equivalent circuit proposed aligns well with the experimental values. As indicated by the DRT analysis, the overall increase in total reaction resistance in the last impedance spectrum is primarily attributed to the rise of charge transfer reaction resistance (P_2) and to some extent the emergence of other processes (P_1 and P_4) that impede the reaction and contribute to the polarization losses. The resulting impedance spectrum can then be fitted using an equivalent circuit with four serial EQ values instead of two.

Subsequently, the DRT results over the entire measurement are plotted in Figure 2e for an in-depth investigation. The low-frequency process P_1 is typical for liquid phase diffusion of reactants,[28−31] presumably dissolved CO_2 or product diffusion in our case.[15] The process is particularly noticeable in the later stage of the experiment with a characteristic frequency ranging from 10^{-1} to 10^0 Hz. During degradation, the increasing peak value and frequency shift indicate a slower effective diffusion of the reactants (Figure 2d). The peak value of P_2, corresponding to the charge transfer resistance, decreases substantially as the electrolyte-wetted area for CO2R simultaneously increases, as evidenced by the corresponding double-layer capacitance C_{dl} during the initial wetting process. At a later stage, the integrated area of P_2 increases again, suggesting growth of the reaction resistance, which occurs alongside a gradual but continuous decrease of C_{dl} (cf. Figure 2e). (Note that all of the retrieved C_{dl} evaluated and discussed outside the context of DRT analysis correspond to P_2.) As mentioned, P_3 is representative of the preceding bicarbonate equilibrium ($CO_2 + OH^- \rightleftharpoons HCO_3^-$), which influences the availability of dissolved CO_2 as electroactive species and thereby contributes to the impedance. Its contribution increases over time, implying that the equilibrium increasingly impedes the reaction, most likely by reducing the availability of dissolved CO_2 as an electroactive species. This will be further discussed below. As for the high-frequency process P_4 (7∼30 kHz), typically, ionic transport[28,29,31−33] and contact impedance[27] are assigned to this frequency range in electrochemical systems. The substantial increase of P_4 at high current density (cf. Figure 3b) along with the related characteristic frequency suggests its association with a transport limitation of ionic

https://doi.org/10.1021/acsenergylett.4c02673
ACS Energy Lett. 2024, 9, 6096−6103

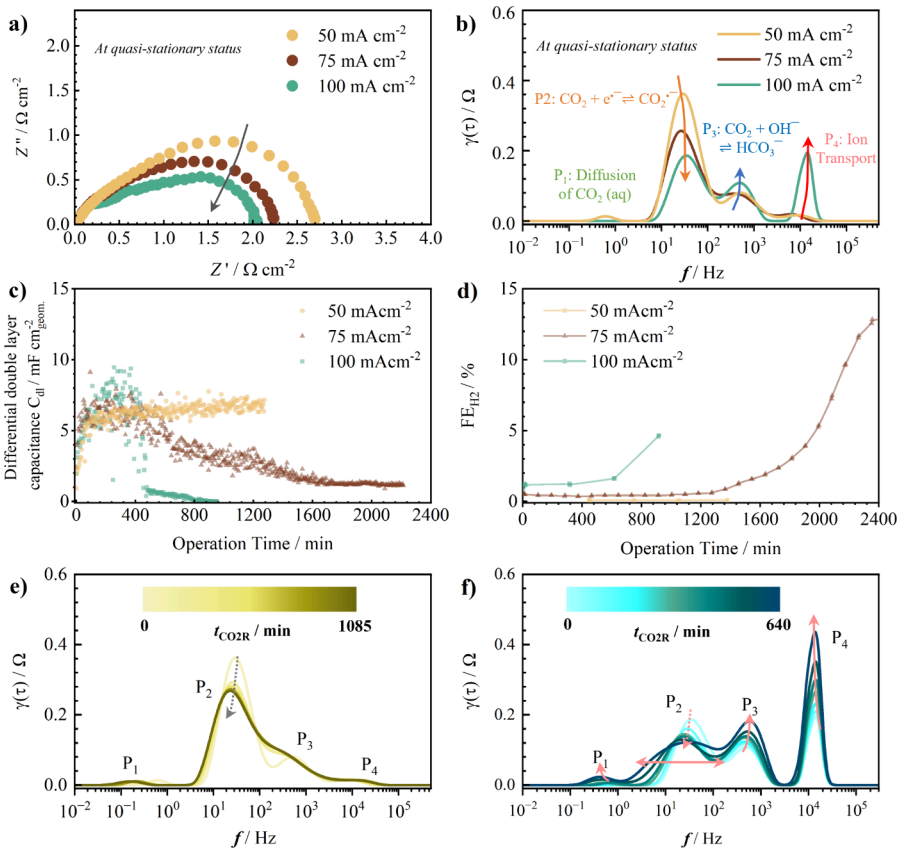

Figure 3. Condition: water bath 12 °C, gaseous backpressure 18 $mbar_g$. (a) Measured and fitted impedance spectra as well as (b) their DRT analysis at the quasi-stationary status at the respective current density. (c) The C_{dl} retrieved by fitting with two serial RQ elements and (d) the Faradaic efficiency of hydrogen produced overtime at various current densities. Computed DRT with identification of distinctive polarization processes overtime at (e) −50 and (f) −100 mA/cm^2.

species and hydroxide (OH^-). This gradual increase at a later stage of the process along with the rise of HER indicates the occurrence or the intensification of a transport limitation during degradation as the derived C_{dl} for the charge transfer reaction from the fitting decreases steadily as well during the reaction (cf. Figure 2f).

As the subsequent step, the impacts of applied current densities on the long-term stability and evolution of DRT were investigated. As illustrated in Figure 3a, the impedance spectra obtained at a quasi-stationary state (after the wetting-in phase and prior to any degradation) at increasing current densities demonstrate a positive and negative correlation with the C_{dl} and the reaction resistance, respectively. In the DRT plot (cf. Figure 3b), peak value P_2 decreases with current,[34,35] while changes of P_1, P_3, and P_4 remain less pronounced, except at high current density (100 $mA{\cdot}cm^{-2}$), where increases of P_3 and P_4 can be observed. At higher current densities, carbonate precipitation is favored, shifting the carbonate equilibrium continuously toward the carbonate side. This shift reduces the availability of free CO_2 in the electrolyte, which in turn slows down the reaction and is observed as an increase in the corresponding resistance of P_3.[15] Meanwhile, the reduction in C_{dl} and the increase in H_2 production takes place at an earlier stage (cf. Figures 3c and 3d). It should be noted that the deviation between fittings using two RQ elements (as done in the beginning) and four RQ elements (suggested by DRT analysis) to derive the C_{dl} value is small (cf. Figure S7). The influence of current density is mainly attributed to an earlier onset of detrimental carbonate precipitation, as increased hydroxide production accelerates its chemical reaction with CO_2 (cf. Figure S8). This blocks the active surface area from the reaction and impedes the transport of the reactants. At 100 $mA{\cdot}cm^{-2}$, a strong correlation exists between the increase in HER and the value of C_{dl}, owing to the rapid degradation (cf. Figure 3d). This is accompanied by an increasing reaction resistance and simultaneous HER at highly negative cathode potentials (cf. Figure S9). In contrast, C_{dl} remains constant at 50 $mA{\cdot}cm^{-2}$ with less apparent carbonate precipitation observed on the GDE surface along with negligible H_2 production throughout the entire measurement (cf. Figures 3d and S10). The corresponding DRT analysis deconvolutes four characteristic peaks for all current densities (P_1, P_2, P_3, and P_4) (cf. Figures 3e and 3f), for which the above assumptions about the underlying processes could be further verified. As can be seen from Figure 3e, for both 50 and 100 $mA{\cdot}cm^{-2}$, the peak area of P_2 initially decreases due to electrowetting; however, for 50 $mA{\cdot}cm^{-2}$, the DRT merely changes afterward. Meanwhile, integrated peak values of P_1, P_3, and P_4 contribute little to the total impedance, showing no obvious increase until the end of the experiment. This indicates that severe degradation does not occur within the investigated time frame. In contrast, the results from the 100 $mA{\cdot}cm^{-2}$ measurement align with those at 75 $mA{\cdot}cm^{-2}$ but show an earlier and more severe onset of degradation. The high resistance at elevated current densities, represented by P_4 from the onset, confirms that a transport limitation for ionic species exists and becomes increasingly problematic, as precipitation blocks transport pathways. To validate the hypothesis about

https://doi.org/10.1021/acsenergylett.4c02673
ACS Energy Lett. 2024, 9, 6096−6103

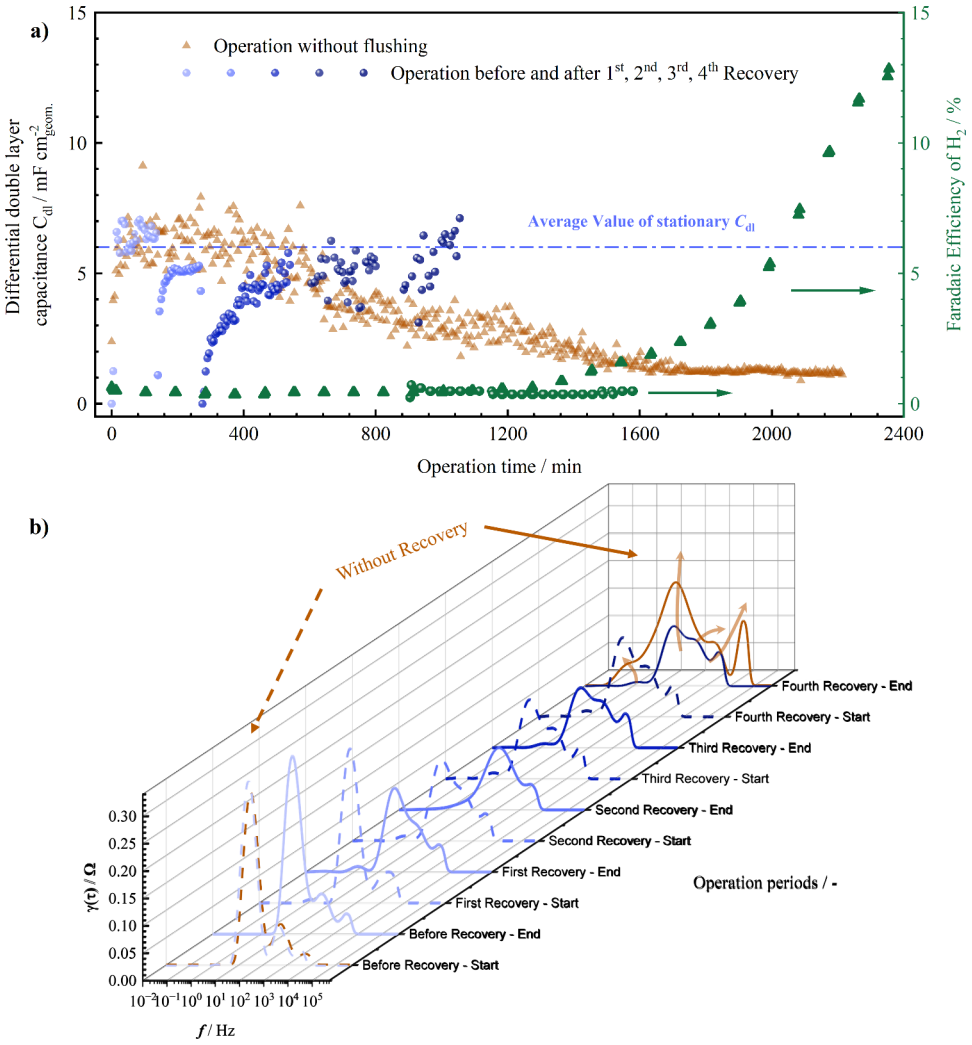

Figure 4. Condition: water bath at 12 °C, −75 mA·cm^{-2}, gaseous backpressure 18 mbar$_g$. (a) Calculated differential double-layer capacitance during the initial run (2 h) and the run after the first (2 h), second (4 h), third (4 h), and fourth (4 h) recovery procedure (light to dark blue dots) compared to the case without recovery (brown triangles). (b) Computed DRT (blue, with; brown, without recovery) over time (dashed line, at the start; solid line, at the end of each measurement).

the relationship among carbonate precipitation, the evolution of C_{dl}, the peaks in the DRT results, and the degradation-induced rise in HER, a series of experiments was devised to study whether an intermediate recovery procedure to dissolve carbonate precipitates can extend the electrolysis time during prolonged electrolysis.

This approach is based on the hypothesis that if degradation stems from carbonate precipitation blocking transport paths and active sites, it should be reversible, allowing the restoration of the initial performance upon removal of the precipitates. For that purpose, the electrolysis at 75 mA/cm^2 with feed through a 12 °C water bath was repeated, but the process was intermittently stopped every 2 or 3 h, during which the cell was disassembled, and the GDE was harvested from the cell. Afterward, the GDE was flushed rigorously with water to dissolve carbonate precipitates within the pores and placed under vacuum before reassembling the cell. After continuing the electrolysis, C_{dl} resumes close to the value where it stopped after a short wetting-in phase (cf. Figure 4a, light to dark blue dots). This remains true as well after this procedure is repeated multiple times. In comparison, in the measurement without the recovery procedure, C_{dl} continuously decreases (cf. Figure 4a, brown triangles). Interestingly, this wetting-in phase (due to potential dependent surface energy reduction at the electrolyte−GDE) cannot be observed after the third repeat of the recovery procedure. It is speculated that the hydrophobic binder PTFE partially decomposes when voltage is applied, as suggested by the previous study,[36] leading to a more hydrophilic GDE surface which facilitates immediate and easier penetration of the electrolyte into the GDE. As a result of the flushing, the lifetime of the GDE could be prolonged compared to the measurement without interruption. While the typical drop of C_{dl} and subsequent increase in H_2 production, which usually occurs with some delay, were not observed within the investigated time frame, both phenomena clearly manifest during continuous electrolysis. The results of DRT analysis shown in Figure 4b indicate that the peak values and areas of all processes in the DRT analysis remain almost constant over time, whereas a substantial change was observed for the same total electrolysis time without intermediate flushing.

For all processes, this is fully consistent with the initial hypothesis that carbonate precipitation is the prevailing degradation mechanism under the system and conditions at

https://doi.org/10.1021/acsenergylett.4c02673
ACS Energy Lett. 2024, 9, 6096−6103

hand. The transport limitation arises due to the blockage of diffusion paths, reaction resistance increases as electrocatalyst accessibility is restrained by the growing volume of salt precipitates, while the equilibrium resistance rises as the availability of free CO_2 drops. It is believed that the carbonate equilibrium is continuously shifted toward the right due to precipitating carbonate species, leaving the equilibrium which in turn leads to sequestration of freely available CO_2 as an active reactant. In contrast, the GDE can maintain its electrochemical active surface area and facilitate efficient transport of gaseous and liquid reactants via a certain recovery procedure. While it is clear that such a recovery procedure is nothing that can be implemented into application (at least not with the electrode architecture utilized here), this approach has proven the capability of using EIS/DRT to monitor the operation of the GDE in long-term experiments, thereby laying the basis for a more thorough systematic operando study.

In conclusion, this research study conceptualized and demonstrated an efficient and stable electrolysis system for CO_2 electroreduction on Bi^0-GDEs in terms of mechanical failure, low amount of hydrogen production (<5%) in the absence of catalyst dissolution, and redistribution under normal operating conditions. By using the distribution of relaxation times (DRT) to analyze electrochemical impedance spectra, we deconvoluted four polarization processes with distinctive time constants and assigned them to specific physical and electrochemical processes based on their correlation to operating conditions, changes over time, and previous work from our group: the electron and ion transport (3k∼300k Hz), the chemical equilibrium of CO_2/HCO_3^- (500−1000 Hz), the charge-transfer process (20−100 Hz), and the diffusion of CO_2 (aq) (0.1−1 Hz). In addition, by combining post-mortem analysis of the peaks' impedance contributions, the frequency shift, and the double-layer capacitance for the charge transfer reaction, we demonstrated how the methodology allows monitoring of the degradation process during long-term operation of CO_2 electroreduction. In our study, this could be mainly attributed to carbonate precipitation with successful attempts to restore the initial performance supporting this hypothesis. While we encourage the community to follow this approach with several open-source tools for DRT available nowadays, we want to stress the importance of using complementary methods (e.g., post-mortem and product quantification) and a thorough design of the experimental procedure to avoid misinterpretation of impedance results. If this is ensured, the presented methodology lends itself for a systematic operando study of long-term stability as a function of operating conditions and GDE properties, thereby advancing this and related technologies forward.

■ ASSOCIATED CONTENT

Supporting Information

The Supporting Information is available free of charge at https://pubs.acs.org/doi/10.1021/acsenergylett.4c02673.

Experimental details (preparation of GDE, REM/EDX, other components, and electrochemical measurements), normal operating conditions, carbonate precipitation, EIS measurement and evaluation (DRT analysis and EIS fitting), and current dependency (PDF)

■ AUTHOR INFORMATION

Corresponding Authors

Dennis Kopljar − *Institute of Engineering Thermodynamics, German Aerospace Center, 70569 Stuttgart, Germany;* orcid.org/0000-0002-2228-2016; Email: Dennis.Kopljar@dlr.de

Kaspar Andreas Friedrich − *Institute of Engineering Thermodynamics, German Aerospace Center, 70569 Stuttgart, Germany; Institute of Building Energetics, Thermal Engineering and Energy Storage, University of Stuttgart, 70569 Stuttgart, Germany;* orcid.org/0000-0002-2968-5029; Email: Andreas.Friedrich@dlr.de

Authors

Qinhao Chen − *Institute of Engineering Thermodynamics, German Aerospace Center, 70569 Stuttgart, Germany; Institute of Building Energetics, Thermal Engineering and Energy Storage, University of Stuttgart, 70569 Stuttgart, Germany;* orcid.org/0000-0002-5871-5426

Alexander Kube − *Institute of Engineering Thermodynamics, German Aerospace Center, 70569 Stuttgart, Germany;* orcid.org/0000-0002-8042-326X

Complete contact information is available at: https://pubs.acs.org/10.1021/acsenergylett.4c02673

Notes

The authors declare no competing financial interest.

■ ACKNOWLEDGMENTS

The authors wanted to thank Rana Bhawna who conducted the SEM and EDX measurements. This work was supported by the funding from the BMWK (Bundesministerium für Wirtschaft und Klimaschutz) in the project AAcid (FKZ 03EE5113F). To improve the readability, certain paragraphs have been refined using ChatGPT during the revision process. Special care was taken during proofreading to ensure the accuracy and correctness.

■ REFERENCES

(1) Wakerley, D.; Lamaison, S.; Wicks, J.; Clemens, A.; Feaster, J.; Corral, D.; Jaffer, S. A.; Sarkar, A.; Fontecave, M.; Duoss, E. B.; et al. Gas diffusion electrodes, reactor designs and key metrics of low-temperature CO2 electrolysers. *Nat. Energy* **2022**, *7* (2), 130−143.

(2) Lai, W.; Qiao, Y.; Wang, Y.; Huang, H. Stability Issues in Electrochemical CO2 Reduction: Recent Advances in Fundamental Understanding and Design Strategies. *Adv. Mater.* **2023**, *35* (51), 2306288.

(3) Leonard, M. E.; Clarke, L. E.; Forner-Cuenca, A.; Brown, S. M.; Brushett, F. R. Investigating Electrode Flooding in a Flowing Electrolyte, Gas-Fed Carbon Dioxide Electrolyzer. *ChemSusChem* **2020**, *13* (2), 400−411.

(4) Sebastián-Pascual, P.; Escudero-Escribano, M. Addressing the Interfacial Properties for CO Electroreduction on Cu with Cyclic Voltammetry. *ACS Energy Letters* **2020**, *5* (1), 130−135.

(5) Nwabara, U. O.; de Heer, M. P.; Cofell, E. R.; Verma, S.; Negro, E.; Kenis, P. J. A. Towards accelerated durability testing protocols for CO2 electrolysis. *Journal of Materials Chemistry A* **2020**, *8* (43), 22557−22571.

(6) Handoko, A. D.; Wei, F.; Jenndy; Yeo, B. S.; Seh, Z. W. Understanding heterogeneous electrocatalytic carbon dioxide reduction through operando techniques. *Nature Catalysis* **2018**, *1* (12), 922−934.

(7) Sun, S.; Mao, Y.; Liu, F.; Zhang, S.; Sun, Y.; Gao, Q.; Liu, X. Recent advances in nanoscale engineering of Pd-based electrocatalysts

for selective CO_2 electroreduction to formic acid/formate. *Energy Materials* **2024**, *4* (2), 400027.
(8) Liu, G.; Li, X.; Liu, M.; Yang, X.; Guo, Z.; Chen, X.; Xu, Q.; Zeng, G.; He, Y. Dimensional engineering of covalent organic frameworks derived carbons for electrocatalytic carbon dioxide reduction. *SusMat* **2023**, *3* (6), 834−842.
(9) Liu, J.; Fu, G.; Liao, Y.; Zhang, W.; Xi, X.; Si, F.; Wang, L.; Zhang, J.; Fu, X.-Z.; Luo, J.-L. Electrochemical conversion of small organic molecules to value-added chemicals and hydrogen/electricity without CO2 emission: electrocatalysts, devices and mechanisms. *eScience* **2024**, 100267.
(10) Qu, D.; Wang, G.; Kafle, J.; Harris, J.; Crain, L.; Jin, Z.; Zheng, D. Electrochemical Impedance and its Applications in Energy-Storage Systems. *Small Methods* **2018**, *2* (8), 1700342.
(11) Dierickx, S.; Weber, A.; Ivers-Tiffée, E. How the distribution of relaxation times enhances complex equivalent circuit models for fuel cells. *Electrochim. Acta* **2020**, *355*, 136764.
(12) Qu, Y.; Yang, K.; Li, W.; Wang, G.; Xiao, L.; Wang, G.; Zhuang, L. Operando Diagnosis of MEA-Type CO2 Electrolyzer via Distribution of Relaxation Times Analysis. *ACS Energy Letters* **2024**, *9* (6), 3042−3048.
(13) Sun, Y.; Bai, F.; Liu, J.; Sun, S.; Mao, Y.; Liu, X.; Huang, Y.; Chen, Y. Identification of Degradation Reasons for a CO2MEA Electrolyzer Using the Distribution of Relaxation Times Analysis. *J. Phys. Chem. Lett.* **2024**, *15* (35), 9122−9128.
(14) Bienen, F.; Kopljar, D.; Geiger, S.; Wagner, N.; Friedrich, K. A. Investigation of CO2 Electrolysis on Tin Foil by Electrochemical Impedance Spectroscopy. *Acs Sustain Chem. Eng.* **2020**, *8* (13), 5192−5199.
(15) Bienen, F.; Kopljar, D.; Lowe, A.; Geiger, S.; Wagner, N.; Klemm, E.; Friedrich, K. A. Revealing Mechanistic Processes in Gas-Diffusion Electrodes During CO2 Reduction via Impedance Spectroscopy. *Acs Sustain Chem. Eng.* **2020**, *8* (36), 13759−13768.
(16) Bienen, F.; Lowe, A.; Hildebrand, J.; Hertle, S.; Schonvogel, D.; Kopljar, D.; Wagner, N.; Klemm, E.; Friedrich, K. A. Degradation study on tin- and bismuth-based gas-diffusion electrodes during electrochemical CO2 reduction in highly alkaline media. *J. Energy Chem.* **2021**, *62*, 367−376.
(17) Vivier, V.; Cachet Vivier, C.; Mezaille, S.; Wu, B. L.; Cha, C. S.; Nedelec, J. Y.; Fedoroff, M.; Michel, D.; Yu, L. T. Electrochemical Study of Bi2 O 3 and Bi2 O 2 CO 3 by Means of a Cavity Microelectrode. I. Observed Phenomena and Direct Analysis of Results. *J. Electrochem. Soc.* **2000**, *147* (11), 4252.
(18) Einerhand, R. E. F.; Visscher, W. H. M.; Barendrecht, E. pH measurement in strong KOH solutions with a bismuth electrode. *Electrochim. Acta* **1989**, *34* (3), 345−353.
(19) Morandi, P.; Flaud, V.; Tingry, S.; Cornu, D.; Holade, Y. Tartaric acid regulated the advanced synthesis of bismuth-based materials with tunable performance towards the electrocatalytic production of hydrogen peroxide. *Journal of Materials Chemistry A* **2020**, *8* (36), 18840−18855.
(20) Chen, Q.; Kube, A.; Schonvogel, D.; Kopljar, D.; Klemm, E.; Friedrich, K. A. Elucidating key mechanistic processes during acidic CO2 electroreduction on gas diffusion electrodes towards stable production of formic acid. *Chemical Engineering Journal* **2023**, *476*, 146486.
(21) Bienen, F.; Paulisch, M. C.; Mager, T.; Osiewacz, J.; Nazari, M.; Osenberg, M.; Ellendorff, B.; Turek, T.; Nieken, U.; Manke, I.; et al. Investigating the electrowetting of silver-based gas-diffusion electrodes during oxygen reduction reaction with electrochemical and optical methods. *Electrochemical Science Advances* **2023**, *3* (1), e2100158.
(22) Brug, G. J.; van den Eeden, A. L. G.; Sluyters-Rehbach, M.; Sluyters, J. H. The analysis of electrode impedances complicated by the presence of a constant phase element. *Journal of Electroanalytical Chemistry and Interfacial Electrochemistry* **1984**, *176* (1), 275−295.
(23) Bienen, F.; Hildebrand, J.; Kopljar, D.; Wagner, N.; Klemm, E.; Friedrich, K. A. Importance of Time-Dependent Wetting Behavior of Gas-Diffusion Electrodes for Reactivity Determination. *Chemie Ingenieur Technik* **2021**, *93* (6), 1015−1019.
(24) Washburn, E. W. The Dynamics of Capillary Flow. *Phys. Rev.* **1921**, *17* (3), 273−283.
(25) Moore, R. C.; Mesmer, R. E.; Simonson, J. M. Solubility of Potassium Carbonate in Water between 384 and 529 K Measured Using the Synthetic Method. *Journal of Chemical & Engineering Data* **1997**, *42* (6), 1078−1081.
(26) Löwe, A.; Schmidt, M.; Bienen, F.; Kopljar, D.; Wagner, N.; Klemm, E. Optimizing Reaction Conditions and Gas Diffusion Electrodes Applied in the CO2 Reduction Reaction to Formate to Reach Current Densities up to 1.8 A cm-2. *Acs Sustain Chem. Eng.* **2021**, *9* (11), 4213−4223.
(27) Ortiz-Quiñonez, J. L.; Vega-Verduga, C.; Díaz, D.; Zumeta-Dubé, I. Transformation of Bismuth and β-Bi2O3 Nanoparticles into (BiO)2CO3 and (BiO)4(OH)2CO3 by Capturing CO2: The Role of Halloysite Nanotubes and "Sunlight" on the Crystal Shape and Size. *Cryst. Growth Des.* **2018**, *18* (8), 4334−4346.
(28) Heinzmann, M.; Weber, A.; Ivers-Tiffée, E. Advanced impedance study of polymer electrolyte membrane single cells by means of distribution of relaxation times. *J. Power Sources* **2018**, *402*, 24−33.
(29) Yuan, H.; Dai, H.; Ming, P.; Wang, X.; Wei, X. Quantitative analysis of internal polarization dynamics for polymer electrolyte membrane fuel cell by distribution of relaxation times of impedance. *Applied Energy* **2021**, *303*, 117640.
(30) Huo, X.; Shan, G.; Yang, L.; Gao, L.; Wang, Y.; Zhang, M.; Fu, Y.; Li, W.; Zhang, J. Impedance analysis of alkaline water electrolysis based on distribution of relaxation time. *Int. J. Hydrogen Energy* **2024**, *53*, 684−697.
(31) Sánchez Batalla, B.; Bachmann, J.; Weidlich, C. Investigation of the degradation of proton exchange membrane water electrolysis cells using electrochemical impedance spectroscopy with distribution of relaxation times analysis. *Electrochim. Acta* **2024**, *473*, 143492.
(32) Giesbrecht, P. K.; Freund, M. S. Investigation of Water Oxidation at IrO2 Electrodes in Nafion-Based Membrane Electrode Assemblies Using Impedance Spectroscopy and Distribution of Relaxation Times Analysis. *J. Phys. Chem. C* **2022**, *126* (42), 17844−17861.
(33) Vanysek, P. Ionic Conductivity and Diffusion at Infinite Dilution. *CRC Hand Book of Chemistry and Physics* **1993**, 5−92.
(34) Barsoukov, E.; Macdonald, J. R. *Impedance spectroscopy: theory, experiment, and applications*; John Wiley & Sons, 2018.
(35) Orazem, M.; Tribollet, B. Model-Based Graphical Methods. *Electrochemical Impedance Spectroscopy* **2008**, 353−362.
(36) Schulze, M.; Christenn, C. XPS investigation of the PTFE induced hydrophobic properties of electrodes for low temperature fuel cells. *Appl. Surf. Sci.* **2005**, *252* (1), 148−153.

https://doi.org/10.1021/acsenergylett.4c02673
ACS Energy Lett. 2024, 9, 6096−6103